Supplementary Information

Formamidinium-based Sn-rich Mixed-halide Perovskite Solar Cells with Near-optimal Bandgap: $FAPb_{1-x}Sn_x(I_{0.8}Br_{0.2})_3$

Yan Chen,[a] Ying Fan Tay,[b] Mingjie Li,[c] Than Zaw Oo,[d] Sing Yang Chiam,[e] Yeng Ming Lam,[f] Tze Chien Sum,[g] and Lydia Helena Wong*[fh]

[a] *School of Materials Science and Engineering, Shandong University, Jinan, Shandong 250061, China*

[b] *Institute of Sustainability for Chemicals, Energy and Environment (ISCE²), Agency for Science, Technology and Research (A*STAR), 1 Pesek Road Jurong Island, Singapore, 627833, Singapore*

[c] *Department of Applied Physics, The Hong Kong Polytechnic University, Kowloon 999077, Hong Kong, China*

[d] *Universities' Research Centre, University of Yangon, Yangon 11041, Myanmar*

[e] *Institute of Materials Research and Engineering, Agency for Science, Technology and Research, 2 Fusinopolis Way, Singapore 138634, Singapore*

[f] *School of Materials Science and Engineering, Nanyang Technological University, 50 Nanyang Avenue, Singapore 639798, Singapore*

[g] *Division of Physics and Applied Physics, School of Physical and Mathematical Sciences, Nanyang Technological University, 21 Nanyang Link, Singapore 637371, Singapore*

[h] *Energy Research Institute @NTU (ERI@N), Research Techno Plaza, X-Frontier Block, 50 Nanyang Drive, Singapore 637553, Singapore*

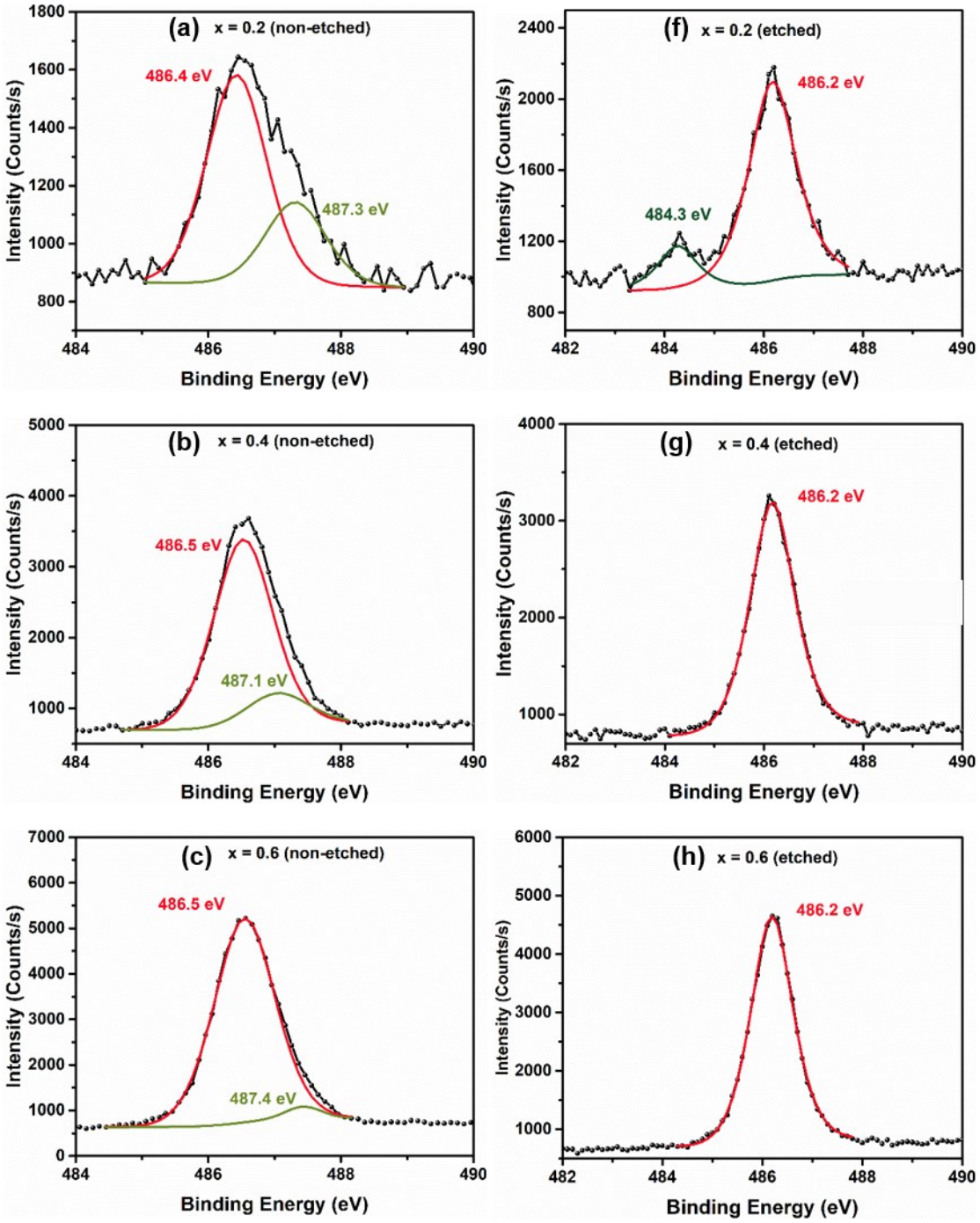

Figure S1 The XPS spectra of Sn 3d5/2 level with fitting for non-etched samples with (a) x = 0.2, (b) x = 0.4, (c) x = 0.6, and for etched samples with (f) x = 0.2, (g) x = 0.4, (h) x = 0.6.

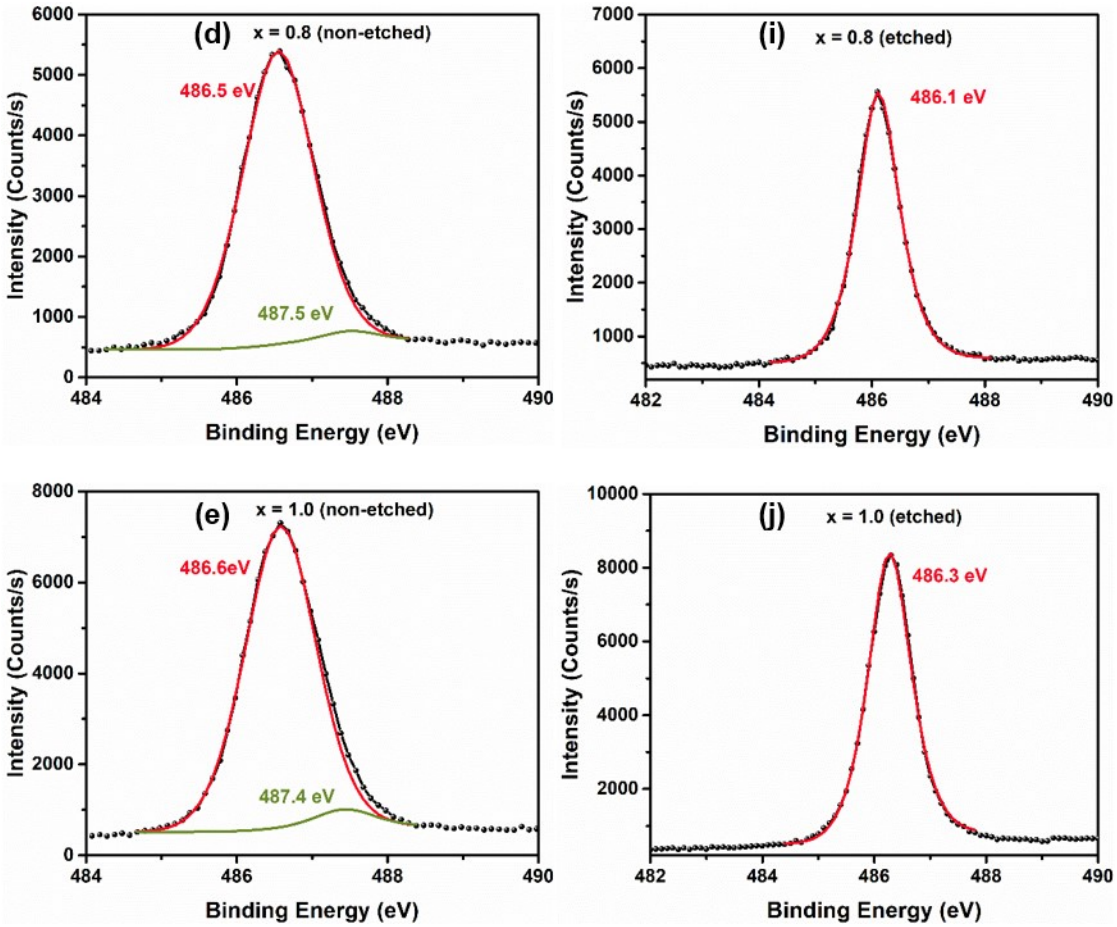

Figure S1 (cont.) The XPS spectra of Sn $3d_{5/2}$ level with fitting for non-etched samples with (d) x = 0.8, (e) x = 1.0 (pure Sn), and for etched samples with (i) x = 0.8, (j) x = 1.0 (pure Sn).

The as-deposited perovskite films were sealed in a N_2 atmosphere bag during transportation and immediately loaded into XPS instrument with minimized air exposure. Nevertheless, the XPS peak of Sn 3d core level for all Sn-containing samples exhibited two chemical states (Sn1 and Sn2) as shown in Figure S2a-e, indicative of air induced oxidation. The chemical state of Sn1 at ~486 eV potentially originates from Sn^{2+} while Sn2 at a higher binding energy of ~487 eV is likely to be Sn-Br oxide.[1] The much lower peak of Sn2 compared to Sn1 implies that Sn oxidation was significantly suppressed owing to the rapid loading process. It is generally known that the elemental composition reflected by XPS correlates with the material within ~10 nm of the surface depth. To further study the elemental composition deeper into the bulk of the samples, argon etching was performed on all the samples until the signal of adventitious Carbon is eliminated. A single chemical state for Sn (at ~486 eV) was identified for all the etched samples with $x \geq$ 0.4, as shown in Figure S2f-j. An additional chemical state at ~485 eV corresponding to Sn^0 was observed in the Sn $3d_{5/2}$ XPS spectrum of x = 0.2 (Figure S2f). The precipitation of Sn could be ascribed to the unreacted PbI_2 left in the x = 0.2 perovskite film, as revealed by its XRD pattern (Figure 1a).

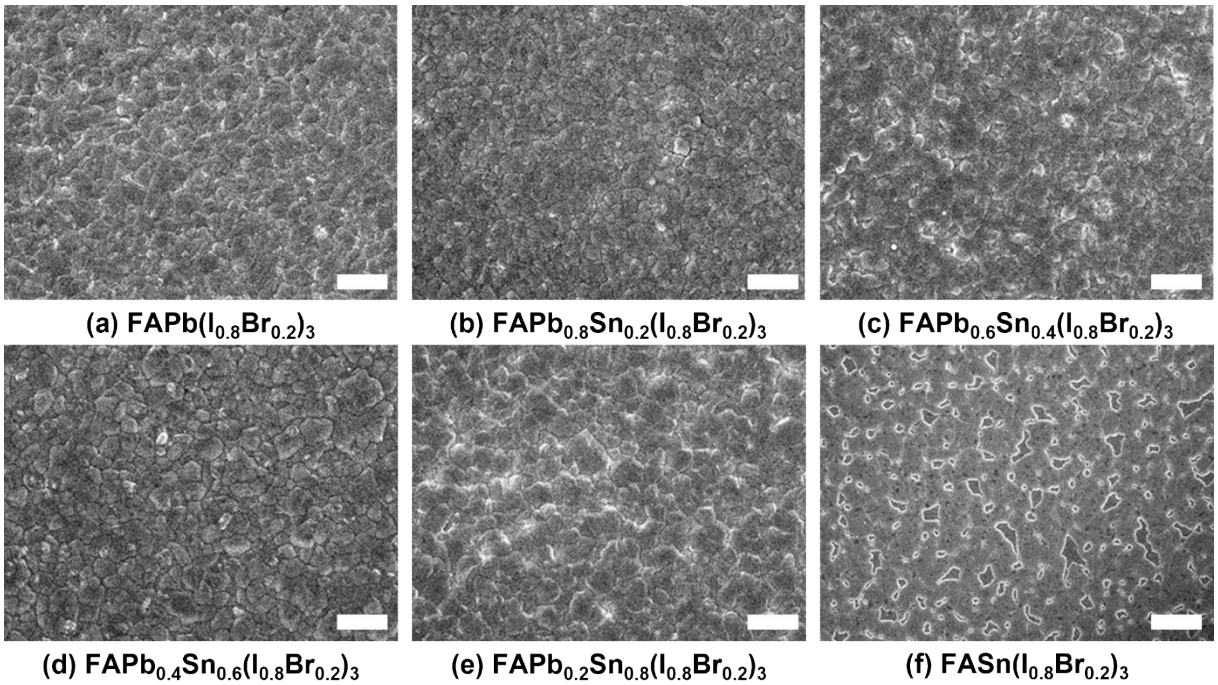

Figure S2 Top-view SEM images of $FAPb_{1-x}Sn_x(I_{0.8}Br_{0.2})_3$ perovskite thin-films depending on the Sn content of: (a) $x = 0$ (pure Pb); (b) $x = 0.2$; (c) $x = 0.4$; (d) $x = 0.6$; (e) $x = 0.8$; (f) $x = 1.0$ (pure Sn). The scale bar in all images is 1 μm.

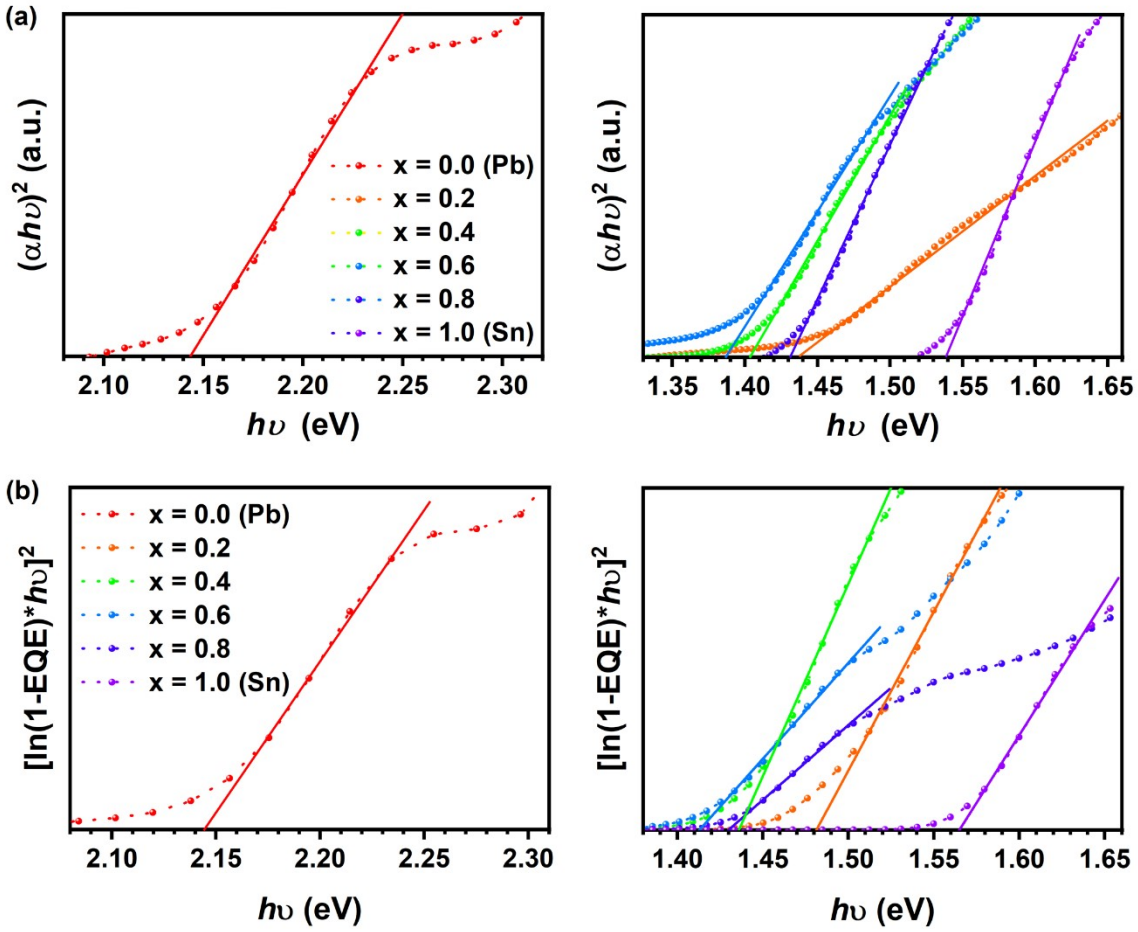

Figure S3 (a) Tauc plot of $(\alpha h\nu)^2$ *versus* $h\nu$ and (b) the plot of $[\ln(1\text{-EQE})\times h\nu]^2$ *versus* $h\nu$ for $FAPb_{1-x}Sn_x(I_{0.8}Br_{0.2})_3$ perovskites.

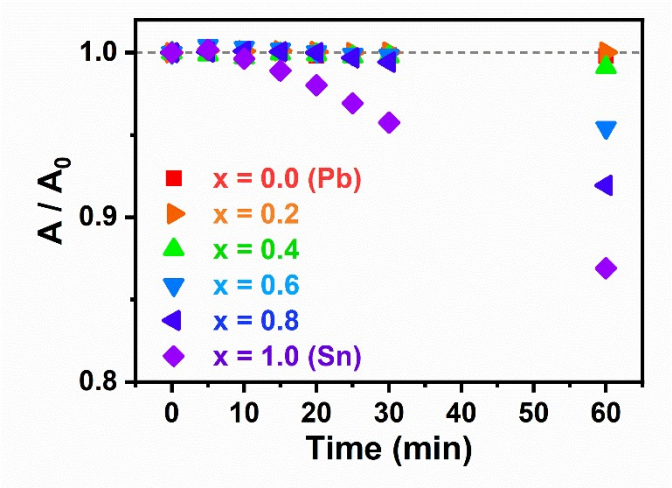

Figure S4 The absorbance at 500nm plotted over time for $FAPb_{1-x}Sn_x(I_{0.8}Br_{0.2})_3$ perovskites. A/A_0 represents the fraction of absorbance remained at 500 nm over time.

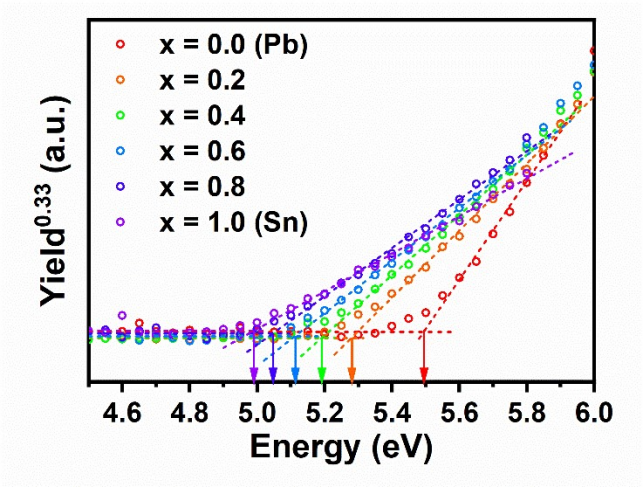

Figure S5 PESA measurement results of $FAPb_{1-x}Sn_x(I_{0.8}Br_{0.2})_3$ perovskites.

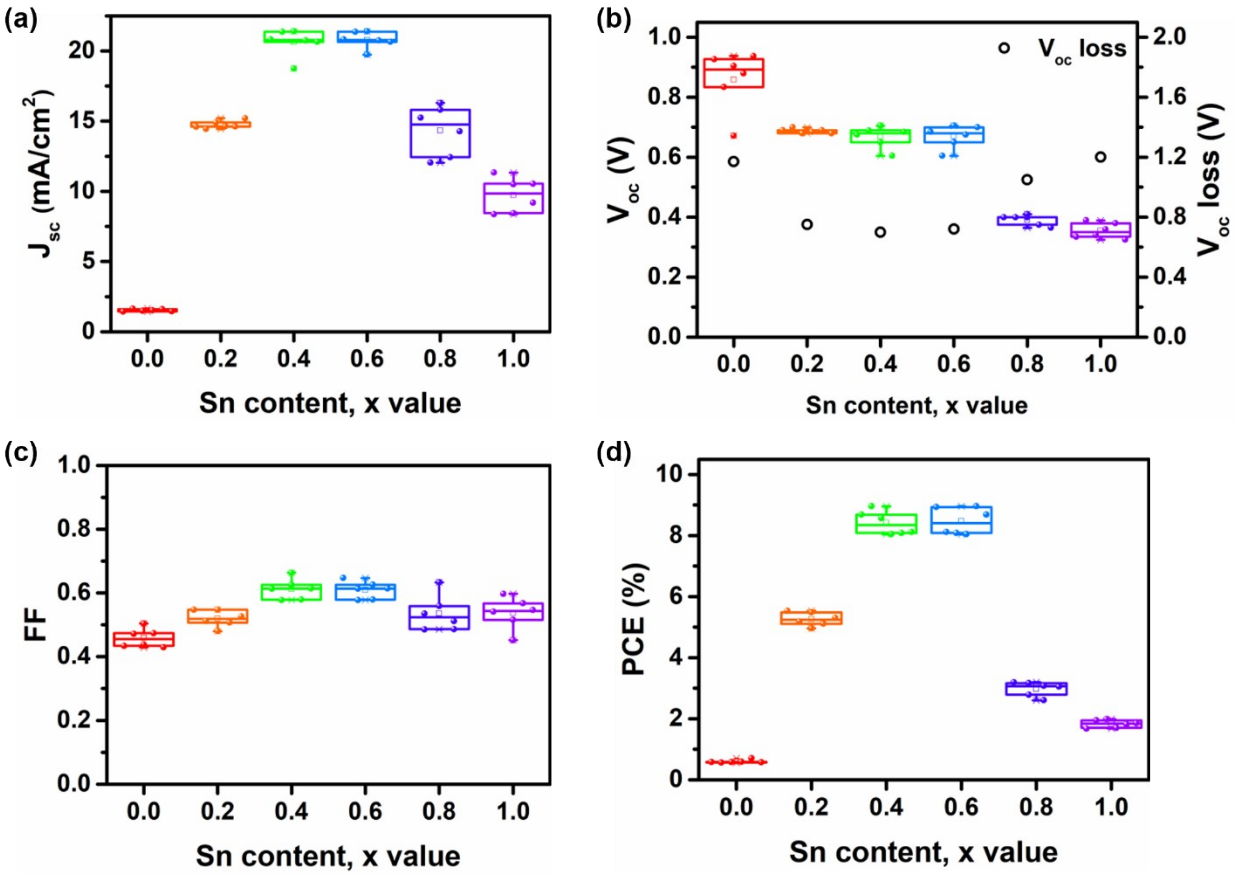

Figure S6 Photovoltaic parameters of $FAPb_{1-x}Sn_x(I_{0.8}Br_{0.2})_3$ based PSCs: (a) J_{sc}, (b) V_{oc}, V_{oc} loss presented as black hollow circles, (c) FF, and (d) PCE.

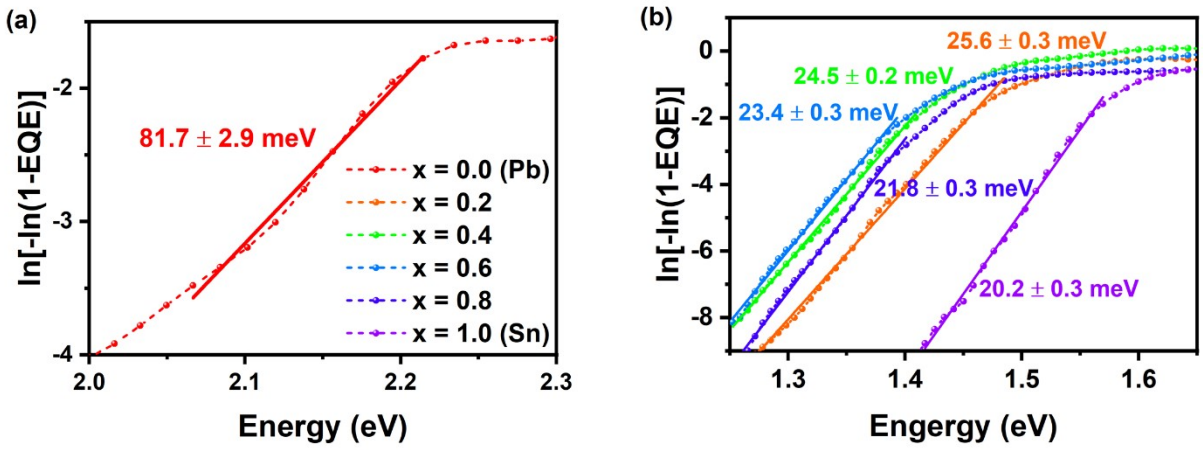

Figure S7 The plot of $\ln[-\ln(1-EQE)]$ against energy for $FAPb_{1-x}Sn_x(I_{0.8}Br_{0.2})_3$ perovskites with (a) $x = 0$, and (b) $x = 0.2 – 1.0$. Urbach energy, E_U, was estimated from the slope of the linear portion near the absorption onset.

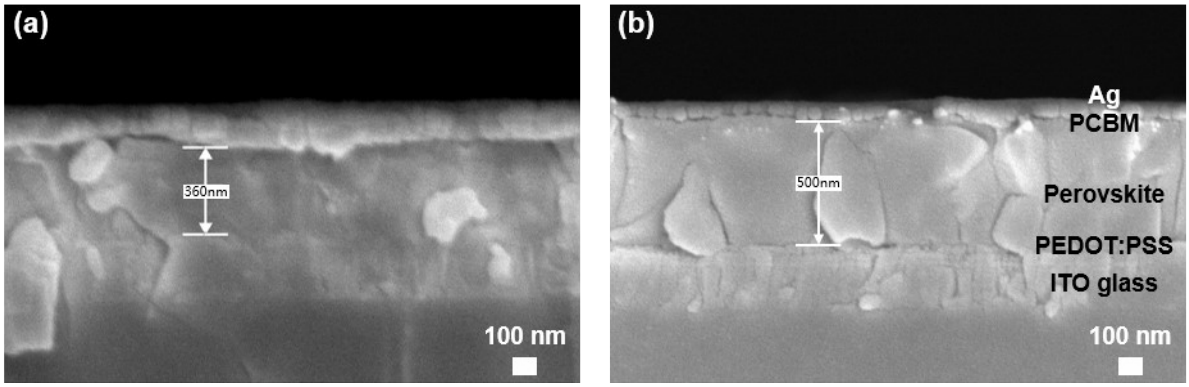

Figure S8 Cross-sectional SEM images of the $FAPb_{0.6}Sn_{0.4}(I_{0.8}Br_{0.2})_3$ PSCs (a) before and (b) after adjusting the concentration of precursor solution. The scale bar in each image is 100 nm.

The thin perovskite layer in Figure S8a was fabricated based on the method described in the Experimental section where the concentration of precursor solution is 1.2 M. Increasing the concentration of precursor solution to 1.5 M resulted in the thick perovskite layer in Figure S8b, while the other processes remained unchanged.

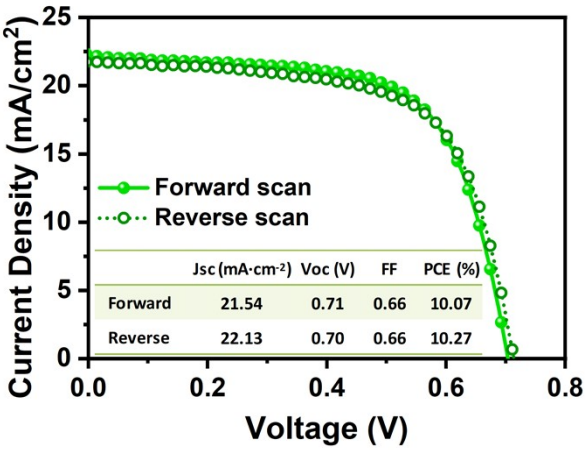

Figure S9 J–V curves of the champion solar cell measured under 100 mW/cm^2 illumination and under forward (solid line) and reverse (dash line) direction. The insets involved its photovoltaic parameters.

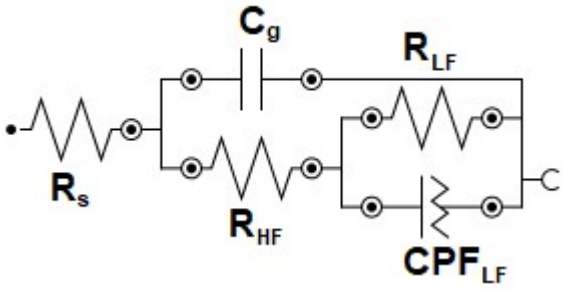

Figure S10 The schematic illustration of the equivalent electrical circuit applied to fit the Nyquist spectra for the $FAPb_{1-x}Sn_x(I_{0.8}Br_{0.2})_3$ based PSCs with x = 0.4 and 0.6. R_s accounts for the series resistance. R_{HF} and C_g correlate to the resistance and geometrical capacitance at the high frequency range of the applied AC signal. R_{LF} and CPE_{LF} contribute to the impedance response at the low frequency range.

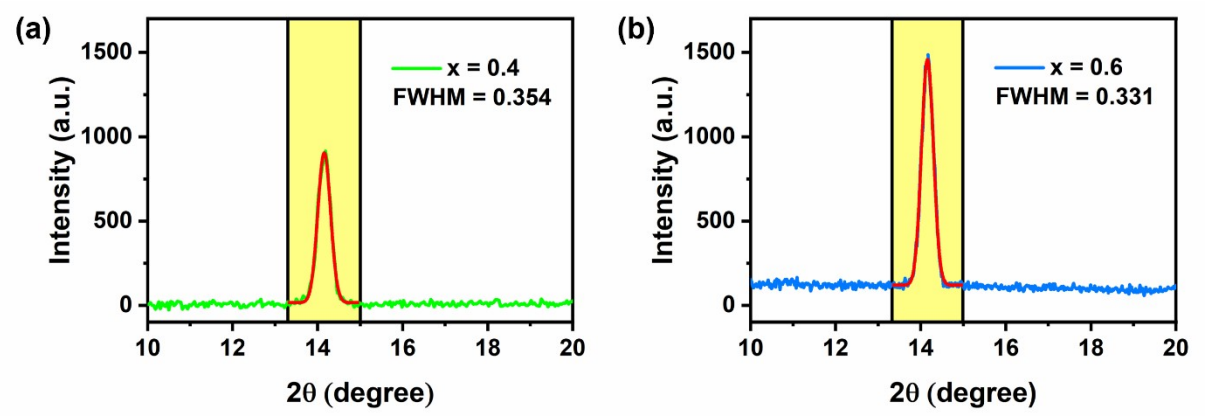

Figure S11 FWHM of the XRD peak at 2θ ≈ 14.12° for (a) x = 0.4 and (b) x = 0.6.

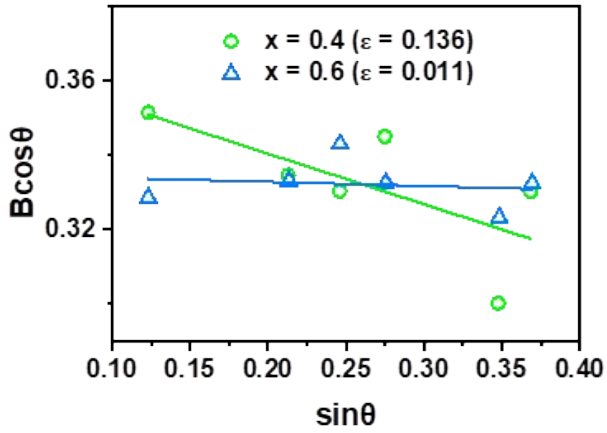

Figure S12 Williamson-Hall plot of $FAPb_{1-x}Sn_x(I_{0.8}Br_{0.2})_3$ perovskites (x = 0.4 and 0.6). The data were calculated using the (100), (110), (200), (210), (222) and (300) peaks from their XRD patterns.

Table S1 Photovoltaic parameters for best-performing PSCs based on $FAPb_{1-x}Sn_x(I_{0.8}Br_{0.2})_3$ (x = 0, 0.2, 0.4, 0.6, 0.8, and 1.0) perovskites.

Sn content / x value	J_{sc} (mA/cm^2)	V_{oc} (V)	FF	PCE (%)	J_{sc} from EQE (mA/cm^2)	V_{oc} loss (V)
0.0 (Pb)	1.58	0.97	0.43	0.66	2.36	1.15
0.2	14.44	0.70	0.55	5.53	14.59	0.74
0.4	19.68	0.70	0.65	8.94	19.03	0.70
0.6	20.39	0.68	0.60	8.36	20.64	0.71
0.8	15.29	0.41	0.51	3.20	16.29	1.02
1.0 (Sn)	11.34	0.34	0.52	1.99	12.17	1.20

Table S2 The capacitive and resistive components (C_g, R_s, R_{HF}, R_{LF} and R_{rec}) obtained from the fitting results of Nyquist spectra for the $FAPb_{1-x}Sn_x(I_{0.8}Br_{0.2})_3$ based PSCs with different Sn contents (x).

x value	C_g (nF)	R_s (Ω)	R_{HF} (kΩ)	R_{LF} (kΩ)	R_{rec} (kΩ)
0.4	8.1	22.9	1.4	6.2	7.6
0.6	8.7	25.6	0.9	4.6	5.5

Table S3 Fitting parameters of TAS spectra for $FAPb_{1-x}Sn_x(I_{0.8}Br_{0.2})_3$ (x = 0.4 and 0.6).

Sn content	λ_{probe} (nm)	A_1	τ_1 (ps)	A_2	τ_2 (ps)	τ_{ave} (ps)
x = 0.4	850	0.46	112 ± 20	0.54	2700 ± 200	1500± 200
x = 0.6	870	0.38	18 ± 4	0.62	4300 ± 400	2700± 300

Reference

1. M.-C. Jung, S. R. Raga and Y. Qi, *RSC Advances*, 2016, **6**, 2819-2825.